Liquid Crystals

ISSN: 0267-8292 (Print) 1366-5855 (Online) Journal homepage: http://www.tandfonline.com/loi/tlct20

Improving the conversion efficiency of an organic distributed feedback laser by varying solvents of the laser gain layer

Minghuan Liu, Yonggang Liu, Guiyang Zhang, Lijuan Liu, Zhihui Diao, Chengliang Yang, Zenghui Peng, Lishuang Yao, Ji Ma & Li Xuan

To cite this article: Minghuan Liu, Yonggang Liu, Guiyang Zhang, Lijuan Liu, Zhihui Diao, Chengliang Yang, Zenghui Peng, Lishuang Yao, Ji Ma & Li Xuan (2016) Improving the conversion efficiency of an organic distributed feedback laser by varying solvents of the laser gain layer, Liquid Crystals, 43:3, 417-426, DOI: 10.1080/02678292.2015.1116628

To link to this article: http://dx.doi.org/10.1080/02678292.2015.1116628

Published online: 11 Jan 2016.

LIQUID CRYSTALS, 2016
VOL. 43, NO. 3, 417–426
http://dx.doi.org/10.1080/02678292.2015.1116628

Taylor & Francis
Taylor & Francis Group

Improving the conversion efficiency of an organic distributed feedback laser by varying solvents of the laser gain layer

Minghuan Liu[a,b], Yonggang Liu[a], Guiyang Zhang[a,b], Lijuan Liu[a,b], Zhihui Diao[a], Chengliang Yang[a], Zenghui Peng[a], Lishuang Yao[a], Ji Ma[a,c] and Li Xuan[a]

[a]State Key Laboratory of Applied Optics, Changchun Institute of Optics, Fine Mechanics and Physics, Chinese Academy of Sciences, Changchun, China; [b]University of Chinese Academy of Sciences, Beijing, China; [c]Liquid Crystal Institute, Kent State University, Kent, OH, USA

ABSTRACT

Control experiments were performed to improve the slope conversion efficiency of the organic distributed feedback laser by varying the dissolution solvents of the laser gain layer, a conjugated polymer poly(2-methoxy-5-(2′-ethyl-hexyloxy)-1,4-phenylene-vinylene) (MEH-PPV) in this work. The distributed feedback configuration of the laser was prepared by holographic photopolymerisation of the polymer/liquid crystal (HPDLC) mixture. Experimental results showed that the tetrahydrofuran (THF) solvent cast laser gain layer had a lower lasing threshold (0.28 μJ/pulse) and a higher slope conversion efficiency (7.8%) than that of the xylene solvent cast laser gain layer (0.5 μJ/pulse, 4.9%). Thin film waveguide characterisation demonstrated that the THF-cast film possessed a smaller waveguide loss (5.3 cm^{-1}) and larger net gain (17.1 cm^{-1}) than the xylene-cast film (8.3 cm^{-1}, 15.7 cm^{-1}). Absorbance and photoluminescence spectra indicated that the THF-cast film showed brighter luminescence at 620 nm and larger absorbance at 532 nm, indicating that the interchain interactions of the MEH-PPV is different, which plays the vital role in improving the optical performance of our organic DFB lasers.

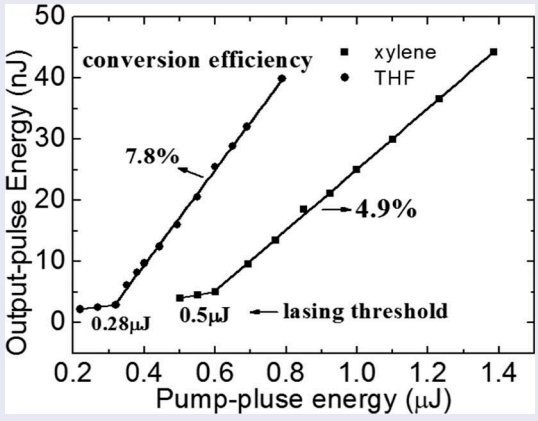

ARTICLE HISTORY
Received 4 September 2015
Accepted 2 November 2015

KEYWORDS
Organic solid-state lasers; distributed feedback; slope conversion efficiency; lasing threshold

1. Introduction

Organic solid-state lasers (OSLs) have received considerable scientific interest since researchers found the lasing from microcavity configurations[1] and the amplification spontaneous emission from waveguide structures[2] with organic semiconducting materials.[3,4] The organic semiconducting materials have merits such as easy fabrication, low-cost, larger scale and outstanding optical properties like pronounced optical absorption and gain throughout the whole visible spectrum. The organic solid-state lasers[5] can also be operated with low oscillation thresholds and capabilities to be tuned across the whole visible range, which would be potentially used in sensors,[6] integrated optics,[7,8] spectroscopies[9,10] and communications.[11]

Compared with organic dyes, organic semiconducting materials have little concentration quenching[12] even in the neat solid thin film. The spin-casting method can be commonly used to fabricate high quality optical polymer thin films with different solvents, such as aromatic chlorobenzene, xylene, toluene and nonaromatic tetrahydrofuran (THF). The conformations of organic conjugated polymers in the solutions will preserve the cast films, and will influence the performance of the final devices.[13]

CONTACT Li Xuan xuanli@ciomp.ac.cn; Ji Ma jma2@kent.edu

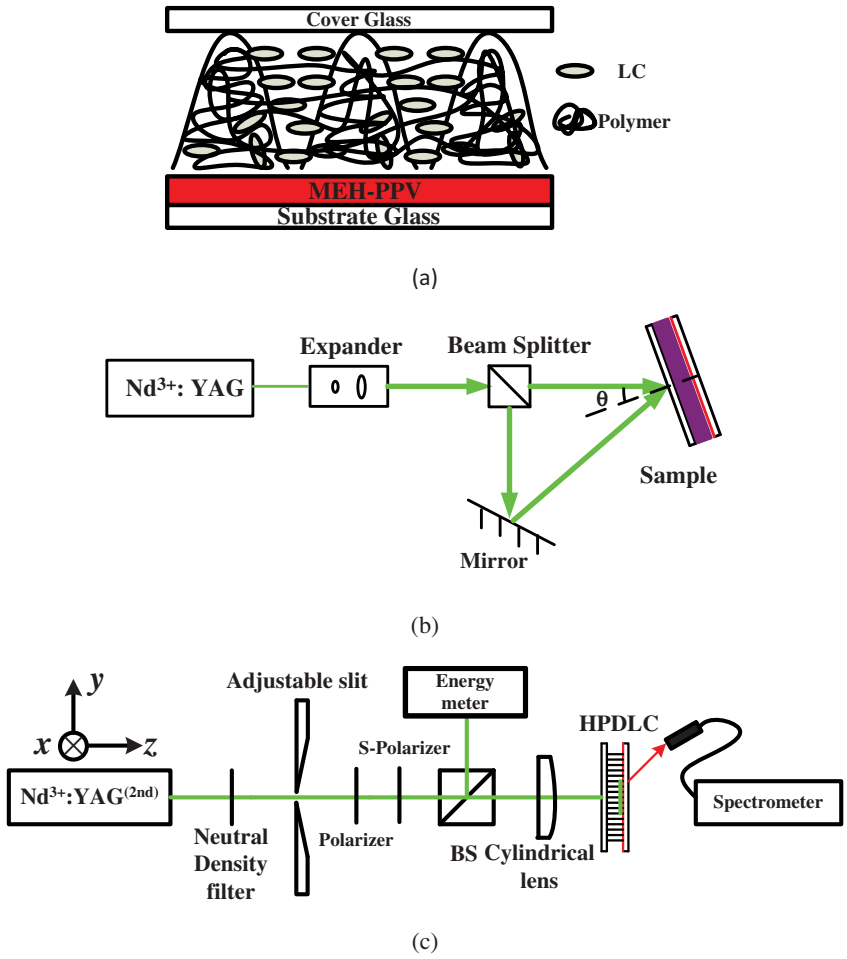

Figure 1. (colour online) (a) Device structure, (b) schematic presentation of the experimental setup for HPDLC grating recording, (c) diagram schematic of lasing pumping.

For example, the performance of polymer light-emitting diodes (LEDs) has been studied by varying solvents, spin speed and annealing properties.[14–18] But, the reports to demonstrate the solvation effect on photoluminescent devices are limited. Therefore, in this work, the performances of the organic solid-state distributed feedback (DFB)[19,20] holographic polymer dispersed liquid crystal (HPDLC) lasers with conjugated polymers as the laser gain layers were investigated by different solvents.

In our DFB HPDLC laser structure, HPDLC transmission grating[21] is used as the DFB configuration cavity because of ease of preparation, low optical scattering[22] and electrical tunability.[23] HPDLC grating contains alternated polymer-rich and LC-rich lamellas, which is prepared in a single-step exposure of a homogeneous mixture of prepolymer/LC mixture to an interference fringe pattern. A laser gain layer was formed by coating poly(2-methoxy-5-(2′-ethyl-hexyloxy)-1,4-phenylene-vinylene) (MEH-PPV) on a glass substrate,[24,25] which was sandwiched between the glass substrate and the HPDLC layer. The HPDLC layer acted as the external feedback configuration, as shown in Figure 1(a).

In recent reports, the slope conversion efficiency[26–30] of the organic DFB laser is from 0.5% to 6.8%. In order to improve this conversion efficiency, we prepared the laser gain, i.e., the organic conjugated polymer MEH-PPV, by spin-casting with different solvents. The effect of the two solvent cast MEH-PPV films was investigated and compared on the device performance.

2. Experimental

2.1. Sample preparation

Ten milligrams of poly(2-methoxy-5-(2′-ethyl-hexyloxy)-1,4-phenylene-vinylene) (MEH-PPV, the chemical structure shown in the inset of Figure 5) (organic light-emitting diode (OLED) Material Tech) were dissolved in THF or xylene solvents by a weight ratio at 0.4 wt.%. The solutions were stirred with a magnetic stirring bar for 48 hours to ensure the sufficient dissolution. A few drops of MEH-PPV solution were used to spin-cast films onto a piece of glass substrate with a dimension of 2.0 by 2.5 cm. The thickness of all MEH-PPV cast films was controlled

at ~80 nm by controlling the spin speed. The thickness of the MEH-PPV film was confirmed using a surface profiler (KLA Tencor P-16+). All experiments were performed under the same ambient conditions.

To form HPDLC as the DFB cavity configuration, a photopolymerisable mixture based on acrylate monomers and liquid crystals were prepared.[31,32] The mixture contained commercially available acrylate monomers (58.8 wt.%) dipentaerythritol hydroxyl pentaacrylate (DPHPA, Aldrich) and phthalic diglycol diacrylate (PDDA, Eastern Acrylic Chem) by a weight ratio of 1:1, nematic liquid crystals TEB30A (n_o = 1.522, Δn = 0.170, Silichem, 29.4 wt.%), crosslinking agent N-vinylpyrrolidone (NVP, Aldrich, 9.8 wt.%), photoinitiator Rose Bengal (RB, Aldrich, 0.5 wt.%) and coinitiator N-phenylglycine (NPG, Aldrich, 1.5 wt.%). The photopolymerisable mixture was injected into an empty cell by capillarity in darkroom after 48 hours of mixing to get a homogeneous mixture. The cell gap was controlled by Mylar spacers at 6 μm. The empty cell was made by two pieces of glass substrates. One had a MEH-PPV coating layer, the other was barely glass. The HPDLC transmission gratings were recorded by illuminating the cells for 30 seconds to the interference pattern created by two s-polarised continuous frequency doubled Nd^{3+}:YAG laser (New Industries Optoelectronics) beams (see Figure 1(b)).[33] The intensity of each beam was about 2.5 mW/cm^2. Ultraviolet (UV) floodlight exposure was performed for the samples using a UV-lamp after holographic recording to provide curing of residual monomers. The mean refractive index of the mixture after photopolymerisation (n_{eff} = 1.545) was measured using an Abbe refractometer (2WA, Kernco). The spatial period (Λ) of the HPDLC grating was controlled by the intersection angle between the writing beams according to:

$$\Lambda = \frac{\lambda_w}{2n_0 \sin(\theta)}, \tag{1}$$

where λ_w is the wavelength of the writing beams, n_0 is the refractive index of air and θ is the half crossing angle of the interference beams in air.

2.2. Lasing characterisation

As shown in Figure 1(c), the samples were optically pumped by a frequency doubled passively Q-switched s-polarised Nd^{3+}:YAG pulsed laser (532 nm, 10 ns, 1–10 Hz repetition rate adjustable) as an excitation source (New Industries Optoelectronics). The pumping laser beam along the sample normal was focused using a cylinder lens (f = 200 mm) to produce a roughly 8 by 1 mm rectangle spot on the sample. An adjustable slit was used to select the central part (4 by 1 mm) of the pump spot to ensure uniform pumping. The emission from the samples was then collected using a fibre-coupled grating spectrometer (Sofn Instruments) with a resolution of ~0.3 nm for the lasing spectra characterisation while the emission was collected using a 50 mm-focal length lens into an energy meter (Coherent) for slope conversion efficiency. Moreover, a non-polarised beam splitter was used in the beam path to split one beam out to monitor the pump beam energy in real time. The wave polarisers and neutral density filter were used to adjust the pump energy continuously to investigate output-pulse energy vs input-pulse energy.

2.3. Pure film characterisation

The absorbance spectra of the cast MEH-PPV film were recorded using a UV-3101PC spectrometer and the photoluminescence of the film was performed at an excitation wavelength of 500 nm using a F-7000FL spectrometer. To ensure that the physical properties were reasonably stable at the time of test, all the samples were aged for 72 hours prior to characterisation.

2.4. Film characterisation by ASE in waveguide

For further investigation of the difference between the THF-cast MEH-PPV film and xylene-cast MEH-PPV film, the film characterisation was performed. In this case, a single beam exposing setup (intensity 10 mw/cm^2, 10 minutes) was used to fabricate a PDLC layer instead of HPDLC on the top surface of the MEH-PPV film to inhibit the oxidisation of the MEH-PPV film when photo pumping as shown in Figure 2. The thin film waveguide amplification of spontaneous emission (ASE) of the PDLC samples was performed similar to that in Section 2.2, except that the emission was collected from the edge of the thin film waveguide.

In such film characterisation, the waveguide losses were determined by measuring the optical loss coefficient from shifting the excitation spot (SES)[34] as shown in Figure 2(a), where the excitation spot was gradually shifted away from the edge of the sample. Assuming that the ASE emission from the end of the excitation spot (I_0) is constant, the emission from the edge of the film should decrease because the spot is translated as a result of the waveguide losses (absorption and scatterings) following the Beer-Lambert law:

$$I = I_0 e^{-\alpha x}, \tag{2}$$

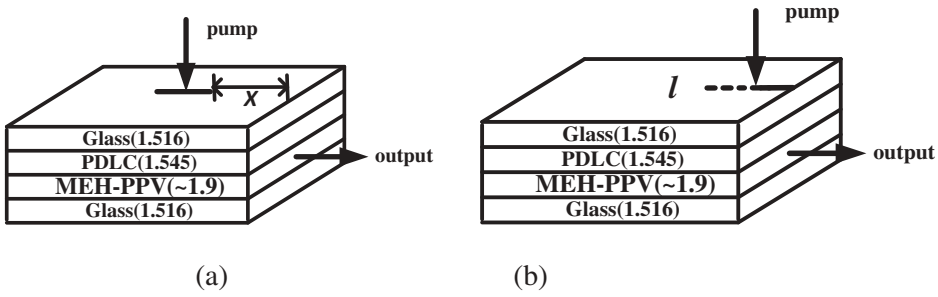

Figure 2. Schematic diagram of how shifting excitation spot (a) and variable stripe length (b) experiments were performed.

where x is the distance between the end of the excitation spot and the edge of the film, α is the waveguide losses, I and I_0 are the ASE emission intensity from the edge of the film and the end of the excitation spot, respectively (Figure 2(a)).

The net gain of the film was obtained by using the variable stripe length (VSL)[35] method, which consists actually of pumping the film with a stripe of variable length and measuring the intensity of the edge-emitted ASE as a function of stripe length as shown in Figure 2 (b). The stripe length was controlled by varying the width of an adjustable slit by means of micrometres. The output intensity from the edge of the stripe should be governed by

$$I(\lambda) = \frac{A(\lambda)I_p}{g(\lambda)}\left(e^{g(\lambda)l} - 1\right), \tag{3}$$

where A is a constant related to the spontaneous emission cross section, I_p is the pumping intensity,g is the net gain coefficient and l is the length of the pumping stripe.

3. Results and discussion

3.1. Lasing properties

According to the Kogelnik formula of the theory of DFB lasers,[19,20] the lasing emission wavelength is

$$\lambda_{las} = \frac{2n_{eff}\Lambda}{m}, \tag{4}$$

where n_{eff} is the effective refractive index of the lasing mode, Λ is the period of the grating and m is the Bragg diffraction order. The lasing wavelength can be tuned by changing the grating period Λ and the effective refractive index n_{eff}. For Bragg diffraction order $m = 3$, taking the value of n_{eff} (1.597[36]) into account, the intersection angle was selected as 54.4° to obtain the lasing wavelength of around 620 nm.

Figure 3(a) shows the lasing spectra of the samples with the cast MEH-PPV film from THF (red line) and xylene (black line) at 3 μJ/pulse pumping energy. Both of the lasing spectra are single mode. The maximum of both spectra is centred at 620.2 nm, which is in agreement with the theoretical calculation from Equation (4). The consistency of the lasing

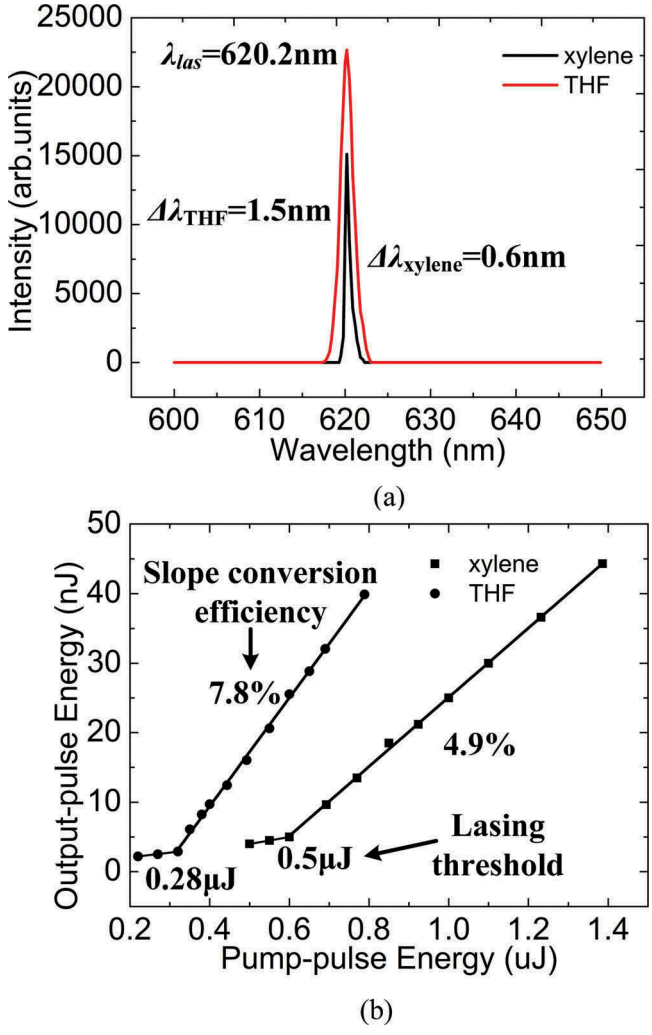

Figure 3. (colour online) (a) Lasing spectra collected at 3 μJ/pulse pumping energy. Red solid line: THF-cast laser; black solid line: xylene-cast laser and (b) output-pulse energy as a function of pump-pulse energy. Circular dots: THF-cast laser; square dots: xylene-cast laser. The solid line is a linear fitting of the data.

wavelength of the THF-cast laser and xylene-cast laser demonstrated the uniformity of the film and device. The linewidth (full width at half maximum) of the lasing spectra was 1.5 and 0.6 nm for the THF-cast laser and the xylene-cast laser, respectively. The reason for the linewidth of the THF-cast laser being larger than that of the xylene-cast laser is that the lasing intensity of the THF-cast laser is two thirds larger than that of the xylene-cast laser at 3 μJ/pulse pumping energy.

Figure 3(b) shows the relationship between pump-pulse energy and output-pulse energy of the lasers. The slope conversion efficiency is defined by the output-pulse energy over the difference of the input-pulse energy and the lasing threshold, which was 7.8% for the THF-cast laser while was 4.9% for the xylene-cast laser. The lasing threshold was 0.28 μJ/pulse for the THF-cast laser and 0.5 μJ/pulse for the xylene-cast laser, respectively. It is shown that the THF-cast laser had a lower lasing threshold and higher slope conversion efficiency. We can see that the different solvent cast laser gain layer gave different optical performance.

3.2. MEH-PPV film spectrum study

Figure 4 displays the absorbance and photoluminescence spectra of the MEH-PPV films cast from THF and xylene solvents. The absorbance spectra line shape was similar, except that the peak is 494 nm for the THF-cast film and 496 nm for the xylene-cast film as shown in Figure 4(a). For photoluminescence spectra, the 0–0 and 0–1 vibrational peak can be easily recognised from the photoluminescence spectra as shown in Figure 4(b). The inset of Figure 4(b) displays energy

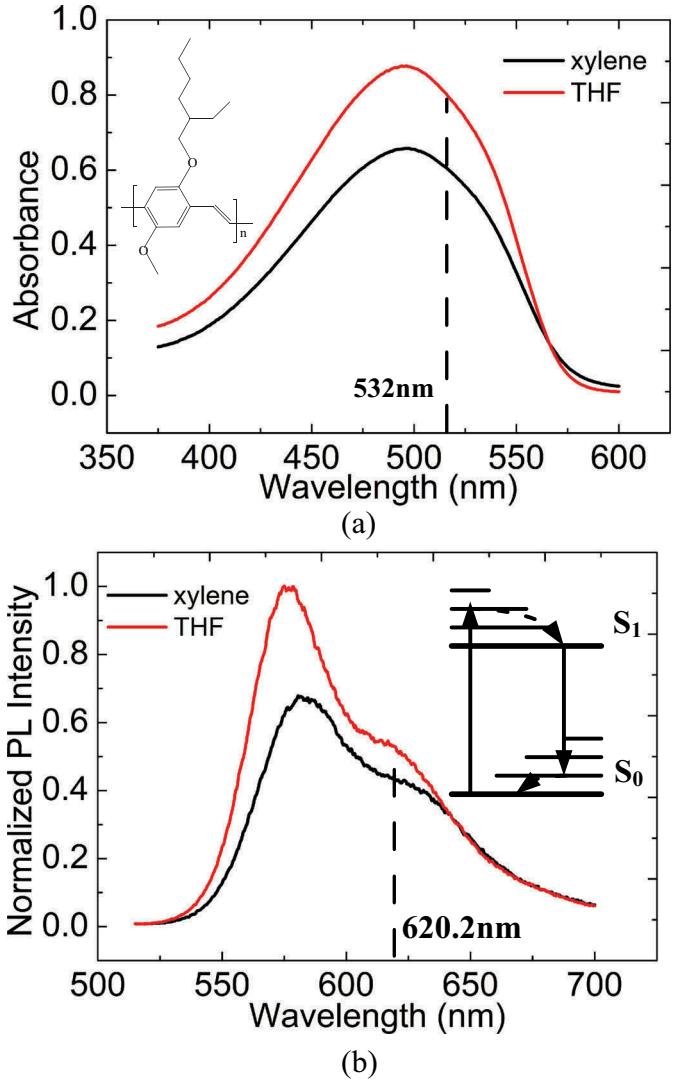

Figure 4. (colour online) Absorbance (a) and normalised photoluminescence (b) spectra of the films cast from xylene (black solid line) and THF (red solid line) solvents. Inset: left panel, chemical structure of MEH-PPV of one repeat unit; right panel, energy levels and transitions of the lowest two singlet states for conjugated polymer molecules.

levels and transitions of the lowest two singlet states for conjugated polymer molecules. The ground state electrons will be excited to the upper energy level when pumping. Then, there will be a fast structural relaxation process. All excited electrons will have a non-radiative transition to $S_{1\text{-}0}$. The excited electrons from $S_{1\text{-}0}$ transit to $S_{0\text{-}0}$ via spontaneous emission, corresponding to the 0–0 vibrational peak while the excited particles from $S_{1\text{-}0}$ transit to $S_{0\text{-}1}$, corresponding to the 0–1 vibrational peak. The 0–0 vibrational peak was 575.2 and 580.6 nm for THF-cast and xylene-cast films, respectively, while the 0–1 vibrational peak of THF-cast and xylene-cast films located at 616.8 and 626.8 nm, respectively. Both the 0–0 and 0–1 vibrational peaks for the xylene-cast film showed red shift in comparison with the THF-cast film. The absorbance and photoluminescence spectra showed some differences between THF-cast and xylene-cast films. However, the difference is small. Therefore, thin film waveguide experiments were performed in the next section to further characterise the properties of the film.

3.3. Film characterisation in waveguide

The refractive index profile of the additional sample which has a PDLC layer on the film of MEH-PPV is displayed as a planar waveguide structure in Figure 2. Hereafter, THF-cast and xylene-cast samples were used to represent films cast from different solvents with a PDLC layer on it. The cover glass and substrate glass have a refractive index of 1.516. The mean value of the PDLC layer is 1.545. The refractive index of MEH-PPV for s-polarised and p-polarised light at 620 nm is ~1.90 and ~1.53, respectively.[37] This anisotropy is a consequence of the polymer chains lying preferentially in the plane of the substrate.[38] Waveguide modelling shows that for a 80 nm-thick film, [34] there is only one TE mode and there are no TM modes.

For a waveguide structure, When the ASE occurs in a long and narrow stripe, most of the light is emitted from the ends of the stripe, because the light is highly amplified if it travels across the full length of the gain region. Therefore, it is a helpful method to collect the light from one end of the pump stripe for characterising the samples in experiment.

Figure 5 shows waveguide ASE spectra of the waveguide structure samples at 12 μJ/pulse pumping energy. Both of the spectra were centred at 620 nm. The spectral linewidths were 7 and 5.5 nm for THF-cast and xylene-cast samples, respectively. It is obvious that the spectral narrowing occurs when the gain overcomes

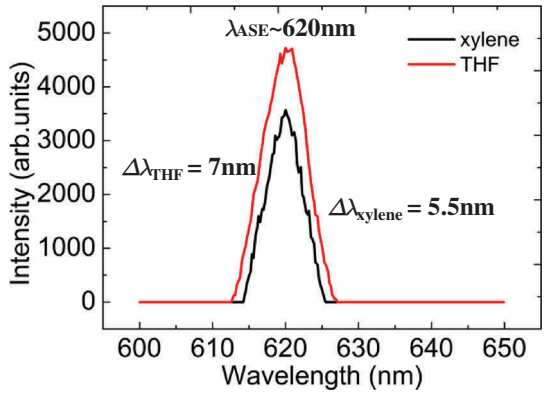

Figure 5. (colour online) ASE spectra collected from the edge of the waveguide samples at a pumping energy of 12 μJ/pulse. Red solid line: THF-cast sample; black solid line: xylene-cast sample.

losses. However, the spectral confinement and selection are inferior for lack of feedback configuration.

Gain and losses are parameters to evaluate a medium such as laser gain layer materials since they are intimately related to the stimulated emission process. Figure 6(a) shows the dependence of the emission intensity at a wavelength of 620 nm with a pumping intensity of 37.5 kW/cm^2. The fitting coefficient of waveguide net gain was 17.1 cm^{-1} for THF-cast and 15.7 cm^{-1} for xylene-cast samples, respectively. Figure 6(b) shows the intensity of light emitted at a wavelength of 620 nm from the edge of the samples at 300 μJ/cm^2. The fitting coefficient of the waveguide losses was 5.3 cm^{-1} for THF-cast and 8.3 cm^{-1} for xylene-cast samples, respectively. In the small-signal regime,[39] considering the gain and losses at the same time:

$$I(z) = I_0 \exp[(g_0 - \alpha)z], \tag{5}$$

where g_0 is the small-signal gain parameter, α is the loss parameter, z is the distance when light travels in the medium, I_0 is the initial intensity of the light and $I(z)$ is the intensity when light travels a distance of z in the medium. It is relatively easy to create the stimulated emission process when losses are small, which means that the lasing threshold is small. A larger gain means that the initial light will be intensely amplified when it travels in the medium. When the initial light travels a distance of 4 mm, the light will be amplified by a factor of 934 in the THF-cast sample and 533 in the xylene-cast sample. Thus, it is understandable that the THF-cast laser has a lower lasing threshold and a higher slope conversion efficiency from the waveguide ASE characterisation.

It is obvious that the THF-cast film has a larger absorbance at 532 nm and brighter photoluminescence at 620.2 nm than the xylene-cast film as shown in

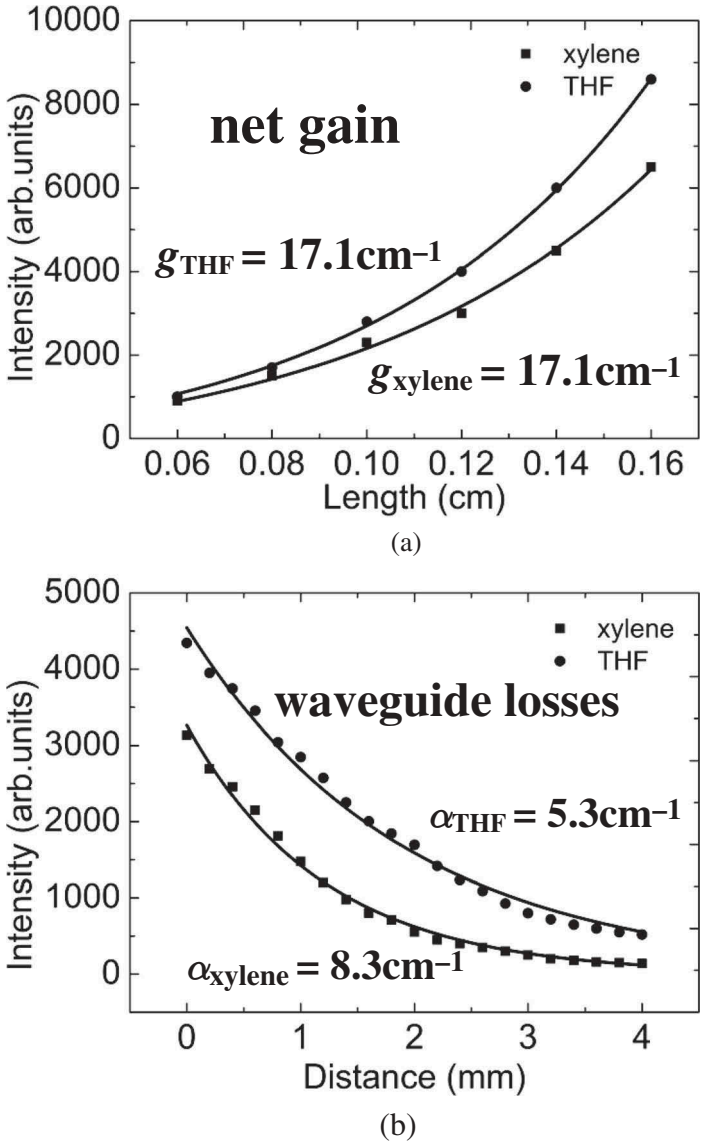

Figure 6. (a) Dependence of the emission intensity at λ = 620 nm with a pumping intensity of 37.5 kW/cm^2 (i.e., 12 μJ/pulse) of the samples. The solid lines are fitting to the data using Equation (3) and (b) the intensity of light emitted at λ = 620 nm from the edge with the distance between the pump stripe end and the sample edge of 300 μJ/cm^2 (i.e., 14 μJ/pulse). The solid lines are exponentially fitted by Equation (2).

Figure 4(a). A larger absorbance means that the ground state electrons will be excited to higher energy level faster, therefore, the population inversion density will be larger. According to the relationship[39]:

$$g = \sigma N, \tag{6}$$

where g is the gain, σ is the stimulated emission cross section and N is the population inversion density. The gain of a material is proportional to the population inversion density when the stimulated emission cross section is constant. It is understandable that the THF-cast sample has a larger gain than the xylene-cast sample.

From the above investigation, we deduce that the dramatic difference of the device performance from different solvent cast MEH-PPV films is from the electronic interactions between the conjugated polymer chains of the cast MEH-PPV film. This electronic interaction can change the packing conformation in the film, further influencing the device performance.[13] When the conjugated polymer chains are dissolved in aromatic solvents (such as xylene), the molecular structure tends to have open straight conformation, allowing chromophores to come into interaction easily as shown in Figure 7(b). On the other hand, when conjugating polymer chains in non-aromatic solvents (such as THF), the molecular structure tends to form tight coils, making it difficult for

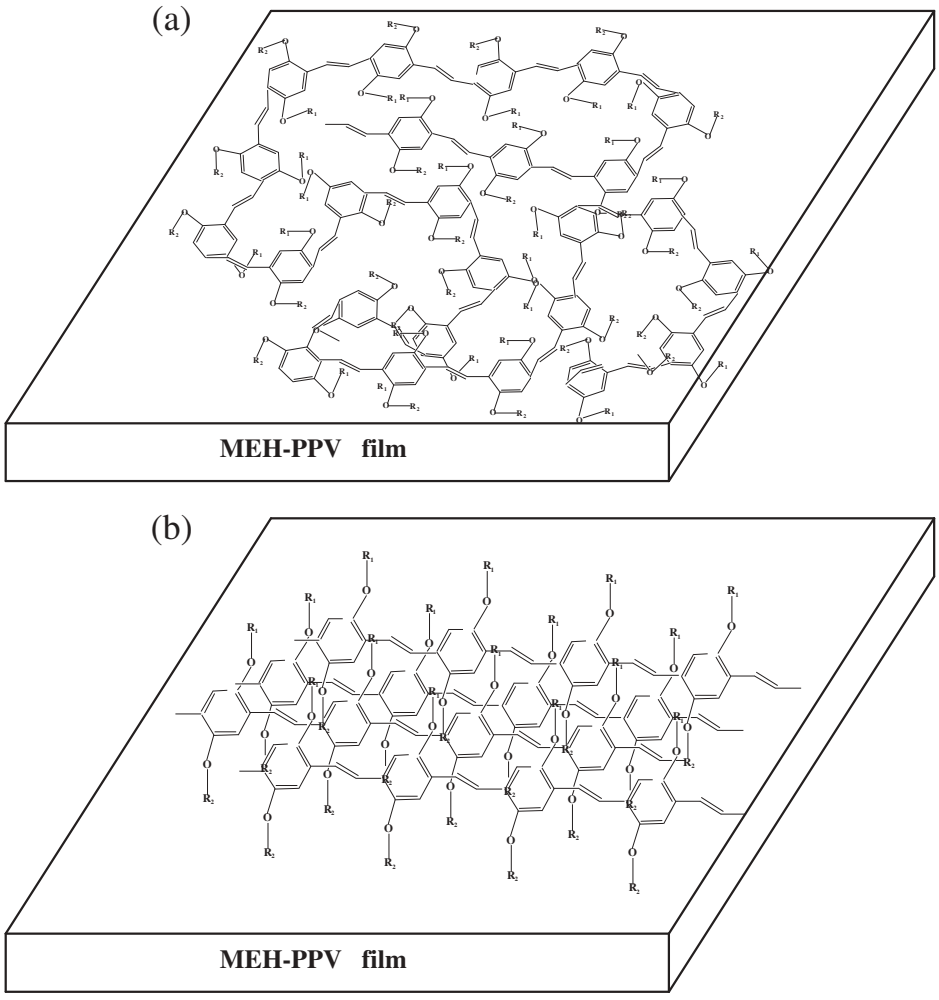

Figure 7. Schematic illustration of MEH-PPV dissolved in (a) THF solvent and (b) xylene solvent.

chromophores to come directly into contact with each other as shown in Figure 7(a). It is generally recognised that conjugated polymer chains can form aggregation, [40,41] which can quench the luminescence, when polymer chains interplay with each other strongly. It is convincing from the experimental results that the aggregation of MEH-PPV chains is promoted in xylene solvent, where the polymer has a more straight conformation, and is restricted in the THF solvent, where the chains tend to form a tighter coil.

4. Conclusions

In conclusion, control experiments were performed by varying the dissolution solvents of the laser gain layer MEH-PPV. The experimental results demonstrate that the organic DFB HPDLC lasers operate better when conjugated polymers dissolved in THF solvent than in xylene. The laser has a lower lasing threshold (0.28 μJ/pulse) and higher slope conversion efficiency (7.8%). The waveguide ASE experiment shows that the THF-cast film has a lower waveguide loss (5.3 cm^{-1}) and higher net gain (17.1 cm^{-1}), which can be used to manifest the better performance of THF-cast lasers. The absorbance and photoluminescence spectra reveal that the absorbance of the THF-cast film is higher at 532 nm, and the photoluminescence is also brighter at 620 nm. These results indicate that the difference in device performance is the consequence of interchain interactions originating from the different dissolution environment. The conjugated polymer interchain interactions play a vital role in improving the performances of photoluminescent devices.

Disclosure statement

No potential conflict of interest was reported by the authors.

Funding

This work was supported by the National Natural Science Foundation of China [61377032, 61378075, 11174274 and 11204299].

References

[1] Tessler N, Denton GJ, Friend RH. Lasing from conjugated-polymer microcavities. Nature. 1996;382:695–697. DOI:10.1038/382695a0.

[2] Hide F, DiazGarcia MA, Schwartz BJ, et al. Semiconducting polymers: A new class of solid-state laser materials. Science. 1996;273:1833–1836. DOI:10.1126/science.273.5283.1833.

[3] Xin H, Li B. Optical orientation and shifting of a single multiwalled carbon nanotube. Light Sci Appl. 2014;3:e205. DOI:10.1038/lsa.2014.86.

[4] Liao C, Slipchenko MN, Wang P, et al. Microsecond scale vibrational spectroscopic imaging by multiplex stimulated Raman scattering microscopy. Light Sci Appl. 2015;4:e265. DOI:10.1038/lsa.2015.38.

[5] Samuel IDW, Turnbull GA. Organic semiconductor lasers. Chem Rev. 2007;107:1272–1295. DOI:10.1021/cr050152i.

[6] Yang Y, Turnbull GA, Samuel IDW. Sensitive explosive vapor detection with polyfluorene lasers. Adv Funct Mater. 2010;20:2093–2097. DOI:10.1002/adfm.200901904.

[7] Vannahme C, Klinkhammer S, Kolew A, et al. Integration of organic semiconductor lasers and single-mode passive waveguides into a PMMA substrate. Microelectron Eng. 2010;87:693–695. DOI:10.1016/j.mee.2009.12.077.

[8] Vannahme C, Klinkhammer S, Lemmer U, et al. Plastic lab-on-a-chip for fluorescence excitation with integrated organic semiconductor lasers. Opt Express. 2011;19:8179–8186. DOI:10.1364/OE.19.008179.

[9] Klinkhammer S, Woggon T, Vannahme C, et al. Optical spectroscopy with organic semiconductor lasers. Org Photon Iv. 2010;7722:77221l.

[10] Woggon T, Klinkhammer S, Lemmer U. Compact spectroscopy system based on tunable organic semiconductor lasers. Appl Phys B. 2010;99:47–51. DOI:10.1007/s00340-010-3953-6.

[11] Clark J, Lanzani G. Organic photonics for communications. Nature Photon. 2010;4:438–446. DOI:10.1038/nphoton.2010.160.

[12] Cornil J, Beljonne D, Calbert J-P, et al. Interchain interactions in organic π-conjugated materials: Impact on electronic structure, optical response, and charge transport. Adv Mater. 2001;13:1053–1067. DOI:10.1002/1521-4095(200107)13:14<1053::AID-ADMA1053>3.0.CO;2-7.

[13] Nguyen T-Q, Doan V, Schwartz BJ. Conjugated polymer aggregates in solution: Control of interchain interactions. J Chem Phys. 1999;110:4068–4078. DOI:10.1063/1.478288.

[14] Liu J, Shi Y, Ma L, et al. Device performance and polymer morphology in polymer light emitting diodes: The control of device electrical properties and metal/polymer contact. J Appl Phys. 2000;88:605–609. DOI:10.1063/1.373799.

[15] Shi Y, Liu J, Yang Y. Device performance and polymer morphology in polymer light emitting diodes: the control of thin film morphology and device quantum efficiency. J Appl Phys. 2000;87:4254–4263. DOI:10.1063/1.373062.

[16] Lee T-W, Park OO. Effect of electrical annealing on the luminous efficiency of thermally annealed polymer light-emitting diodes. Appl Phys Lett. 2000;77:3334–3336. DOI:10.1063/1.1328095.

[17] Lee T-W, Park OO. The effect of different heat treatments on the luminescence efficiency of polymer light-emitting diodes. Adv Mater. 2000;12:801–804. DOI:10.1002/(ISSN)1521-4095.

[18] Nguyen T-Q, Martini IB, Liu J, et al. Controlling interchain interactions in conjugated polymers: the effects of chain morphology on exciton–exciton annihilation and aggregation in MEH–PPV films. J Phys Chem B. 2000;104:237–255. DOI:10.1021/jp993190c.

[19] Shank C, Bjorkholm J, Kogelnik H. Tunable distributed-feedback dye laser. Appl Phys Lett. 1971;18:395–396. DOI:10.1063/1.1653714.

[20] Kogelnik H, Shank CV. Coupled-wave theory of distributed feedback lasers. J Appl Phys. 1972;43:2327–2335. DOI:10.1063/1.1661499.

[21] Sutherland RL, Natarajan LV, Tondiglia VP, et al. Bragg gratings in an acrylate polymer consisting of periodic polymer-dispersed liquid-crystal planes. Chem Mater. 1993;5:1533–1538. DOI:10.1021/cm00034a025.

[22] Huang W, Deng S, Li W, et al. A polarization-independent and low scattering transmission grating for a distributed feedback cavity based on holographic polymer dispersed liquid crystal. J Opt. 2011;13:085501. DOI:10.1088/2040-8978/13/8/085501.

[23] Huang W, Diao Z, Yao L, et al. Electrically tunable distributed feedback laser emission from scaffolding morphologic holographic polymer dispersed liquid crystal grating. Appl Phys Express. 2013;6:022702. DOI:10.7567/APEX.6.022702.

[24] Diao Z, Xuan L, Liu L, et al. A dual-wavelength surface-emitting distributed feedback laser from a holographic grating with an organic semiconducting gain and a doped dye. J Mater Chem C. 2014;2:6177–6182. DOI:10.1039/C4TC00519H.

[25] Liu L, Xuan L, Zhang G, et al. Enhancement of pump efficiency for an organic distributed feedback laser based on a holographic polymer dispersed liquid crystal as an external light feedback layer. J Mater Chem C. 2015;3:5566–5572. DOI:10.1039/C5TC00731C.

[26] Oki Y, Yoshiura T, Chisaki Y, et al. Fabrication of a distributed-feedback dye laser with a grating structure in its plastic waveguide. Appl Opt. 2002;41:5030–5035. DOI:10.1364/AO.41.005030.

[27] Turnbull GA, Andrew P, Barnes WL, et al. Operating characteristics of a semiconducting polymer laser pumped by a microchip laser. Appl Phys Lett. 2003;82:313–315. DOI:10.1063/1.1536249.

[28] Criante L, Lucchetta DE, Vita F, et al. Distributed feedback all-organic microlaser based on holographic polymer dispersed liquid crystals. Appl Phys Lett. 2009;94:111114. DOI:10.1063/1.3103276.

[29] Xia RD, Lai W-Y, Levermore PA, et al. Low-threshold distributed-feedback lasers based on pyrene-cored starburst molecules with 1,3,6,8-attached oligo(9,9-Dialkylfluorene) arms. Adv Funct Mater. 2009;19:2844–2850. DOI:10.1002/adfm.v19:17.

[30] Tsutsumi N, Shinobu M. All organic DFB laser enhanced by intermediate high refractive index polymer layer. Appl Phys B. 2011;105:839–845. DOI:10.1007/s00340-011-4688-8.

[31] Ma J, Huang W, Xuan L, et al. Holographic polymer dispersed liquid crystals: From materials and morphologies to applications. In: Jain V, Kokil A, editors. Optical properties of functional polymers and nano engineering applications. Roca Raton (FL): CRC; 2014.
[32] Diao Z, Huang W, Peng Z, et al. Anisotropic waveguide theory for electrically tunable distributed feedback laser from dye-doped holographic polymer dispersed liquid crystal. Liq Cryst. 2014;41:239–246. DOI:10.1080/02678292.2013.851289.
[33] Diao Z, Deng S, Huang W, et al. Organic dual-wavelength distributed feedback laser empowered by dye-doped holography. J Mater Chem. 2012;22:23331–23334. DOI:10.1039/c2jm35437c.
[34] Negro LD, Bettotti LP, Cazzanell M, et al. Applicability conditions and experimental analysis of the variable stripe length method for gain measurements. Opt Commun. 2004;229:337–348. DOI:10.1016/j.optcom.2003.10.051.
[35] McGehee MD, Heeger AJ. Semiconducting (conjugated) polymers as materials for solid-state lasers. Adv Mater. 2000;12:1655–1668. DOI:10.1002/(ISSN)1521-4095.
[36] Huang W, Diao Z, Liu Y, et al. Distributed feedback polymer laser with an external feedback structure fabricated by holographic polymerization technique. Org Electron. 2012;13:2307–2311. DOI:10.1016/j.orgel.2012.07.004.
[37] Tammer M, Monkman AP. Measurement of the anisotropic refractive indices of spin cast thin poly(2-methoxy-5-(2′-ethyl-hexyloxy)-p-phenylenevinylene) (MEH-PPV) films. Adv Mater. 2002;14:210–212. DOI:10.1002/(ISSN)1521-4095.
[38] McBranch D, Campbell IH, Smith DL, et al. Optical determination of chain orientation in electroluminescent polymer-films. Appl Phys Lett. 1995;66:1175–1177. DOI:10.1063/1.113848.
[39] Zhou B, Gao Y, Chen T, et al. Principles of Lasers. 6th ed. Peking: National Defend Industry Press; 2008.
[40] Jakubiak R, Collison CJ, Wan WC, et al. Aggregation quenching of luminescence in electroluminescent conjugated polymers. J Phys Chem. 1999;103:2394–2398. DOI:10.1021/jp9839450.
[41] Huser T, Yan M. Aggregation quenching in thin films of MEH-PPV studied by near-field scanning optical microscopy and spectroscopy. Synth Met. 2001;116:333–337. DOI:10.1016/S0379-6779(00)00432-X.